9-2017

A sustainable approach for tungsten carbide synthesis using renewable biopolymers

Monsur Islam
Clemson University

Rodrigo Martinez-Duarte
Clemson University, rodrigm@clemson.edu

A sustainable approach for tungsten carbide synthesis using renewable biopolymers

Monsur Islam and Rodrigo Martinez-Duarte*

Multiscale Manufacturing Laboratory, Department of Mechanical Engineering, Clemson University, Clemson, SC, USA

Abstract

Here we present a sustainable, environment-friendly and energy-efficient approach for synthesis of porous tungsten carbide (WC). A biopolymer-metal oxide composite featuring iota-carrageenan, chitin and tungsten trioxide (WO_3) was used as the precursor material. The reaction mechanism for the synthesis of WC was estimated using the results from X-ray diffraction characterization (XRD). A synthesis temperature of 1300 ºC and dwell time of 3 hours were found to be the optimum process parameters to obtain WC >98% pure. The grain size, porosity and Brunauer–Emmett–Teller (BET) surface area of the synthesized WC were characterized using field emission scanning electron microscopy, high resolution transmission electron microscopy and nitrogen adsorption-desorption. A mesoporous WC was synthesized here with a grain size around 20 nm and BET surface area of 67.03 m^2/g. Gel casting was used to demonstrate the manufacturing capability of the proposed precursor material. The WC obtained after heat treatment preserved the original shape albeit significant shrinkage. The WC synthesized here has potential applications in high temperature filters, catalysis, fuel cells and batteries.

Keywords: Tungsten carbide; Renewable biopolymers; Carbon; Porous; Molding.

1. Introduction

Tungsten carbide (WC) features some unique properties such as high melting point, high electrical conductivity, high hardness, low friction coefficient, high chemical stability and high oxidation resistance [1–3]. These properties enabled the use of WC in applications such as machining tools, filters, catalysts [4], fuel cells [5], batteries [6] and erosion resistant materials for aerospace components [7]. In particular, porous WC is widely used in filter applications under harsh environments, catalysis and fuel cells [8–13]. The worldwide production of WC is approximately 3900 metric tons [14]. The large majority of the industrial production of WC relies on the carbothermal reduction reaction (CRR). This reaction uses an excess of carbon and an inert atmosphere to reduce metal oxides to metals and then react them with carbon to generate their carbide [15,16]. Unfortunately, the current sources of carbon in the CRR method are non-renewable and include carbon black, coke, asphalt or graphite. These are usually extracted from oil, mined, and their obtainment demands a significant amount of energy [17–20]. In particular, the derivation of the 2 million metric tons of carbon black required in the United States every year translates to a consumption of around 450 million gallons of

* Corresponding author: Tel: +1 864-353-7856. Email: rodrigm@clemson.edu (Rodrigo Martinez-Duarte)

petroleum oil [21–23]. Such high demand comes from different industries such as carbide manufacturing and tire production. Hence, there is a need to incorporate renewable resources as the carbon source in carbide manufacturing. To this end, we present the use of renewable carrageenan and chitin as the carbon source in the synthesis of WC. These are biopolymers derived from algae and disposed shrimp shells respectively. We mix these biopolymers with tungsten oxide nanoparticles to derive a gel-like paste that will serve as carbide precursor. Furthermore, we use molding to shape this carbide precursor. Heat treatment of these shapes at increasing temperatures leads to carbonization of the biopolymer, oxide reduction into metal and eventually carbide formation. In this work, we focus our study on two process parameters: a) composition of the carbide precursor, and b) heat treatment. We also demonstrate the molding of the precursor to obtain multi-scale structures. By optimizing composition and heat treatment, we aim at developing a carbide synthesis process that is environmentally friendly, sustainable and energy-efficient. Molding can enable a manufacturing process of economic, sustainable pieces with potential application in filtering under harsh environments and high temperatures as well as catalysis.

We build upon previous reports on the use of biopolymers as the carbon source for the synthesis of carbides. For example, Prener and Schenectady demonstrated the use of sucrose as the carbon precursor to form silicon carbide [24]. Schnepp et al. adopted the gelation route to synthesize iron carbide using gelatin and chitosan gel as the precursor material [25]. To date, synthesis of WC has been demonstrated using only chitosan as the carbon source [26,27]. Here we use a biopolymer composite of chitin, carrageenan and tungsten oxide nanoparticles as a carbide precursor. Carbonization of carrageenan and chitin leads to the formation of micro- and mesoporous carbon with high specific surface area [28,29] which is expected to yield better interaction with the metal precursor during the CRR. In terms of manufacturability, this biopolymer composite features rigid gel-like properties while dissolved in water [30], which is suitable for manufacturing technology such as molding and additive manufacturing. Besides facilitating its shaping, the tunable rheology of the biopolymer composite can also help to optimize dispersion of the metal precursor homogeneously in the composite matrix, leading to a more uniform carbide.

In this study, we first address the impact of the precursor composition and heating parameters on grain size and porosity of the final material. We aim at understanding this relation to optimize the time and energy required to synthesize a desired material. In the last section, we demonstrate the molding of the carbide precursor into shapes of different scale.

2. Experimental Section

2.1 Materials and Reagents

Iota-carrageenan (IC) (catalog number: C1138) and chitin from shrimp shells (catalog number: C9213) were purchased from Sigma Aldrich, USA. High purity tungsten oxide (WO_3) nanoparticles of 23-65 nm diameter were purchased from US Research Nanomaterials, Inc (catalog number: US3540). All materials were used as received. Ultra-pure water was used for the preparation of the polymer composite.

2.2 Experimental Method

Dried powders of IC and chitin were manually mixed in a weight ratio of 1:4 to ensure intermolecular binding of IC and chitin [31]. WO_3 nanoparticles were then added to the powder mix to obtain a WO_3:C ratio of 1:6, and vortexed for 10 minutes (Thermo Scientific, Maximix M16710-33Q). Although a ratio of 1:4 WO_3:C is theoretically required [32], other authors have reported the need for a 1:6 ratio to ensure the occurrence of a carbothermal reduction reaction [33]. The exact amount of WO_3 to be added to the biopolymer mix was deduced based on the carbon yield from the biopolymer mix detailed in the results section below. Once the biopolymers and WO_3 were appropriately mixed, 5 g of this powder mixture were added to 15 ml of ultra-pure water and manually mixed using a spatula. The resultant material resembles a gel and will be referred to as the polymer composite precursor (PCP).

The PCP was heat treated at different temperatures ranging from 750 °C to 1450° C in an alumina tube furnace (TF1400 or TF1700, Across International, USA) under a constant nitrogen gas flow rate of 10 SCFH (Standard Cubic Feet per Hour). The heating protocol consisted of 5 steps: (a) heat from room temperature to 300 °C at a rate of 5 °C/min; (b) dwell at 300 °C for 30 minutes to eliminate excess oxygen from the tube; (c) heat from 300 °C to final temperature at 5 °C/min; (d) dwell at the final temperature for a specific time and finally (e) cool down to room temperature by turning off the furnace. The final temperature and dwell time at this temperature were parameters of study in this work.

To investigate the molding capability of the PCP and the obtainment of porous carbide forms, we used polycarbonate molds machined in-house (GX minimill, Minitech Machinery Corporation, USA). The molds featured circular and square cross sections ranging in characteristic length from 1 mm to 9 mm. After molding, the PCP was dried at 90 °C for 2 hours in the tube furnace. This enabled a clean de-molding step to obtain free standing parts of PCP xerogel. The shaped xerogel was heat treated in a nitrogen atmosphere following the same heating protocol detailed above. The dimensions of the PCP, xerogel and material resulting from the heat treatment were measured using a digital caliper.

2.3 Characterization

Thermogravimetric analysis (TGA) was performed for the IC-chitin biopolymer complex without the nanoparticles at 1000 °C under nitrogen gas flow with a heating rate of 5 °C/min to investigate the carbon yield of such a mixture. The crystallinity and composition of the carbonaceous materials obtained after heat treatment were characterized by X-ray diffraction (XRD) spectroscopy using Cu-Kα radiation (Rigaku Ultima IV, Japan). Material correlation was performed using the International Centre for Diffraction Database (ICDD). The morphology and elemental analysis of the carbonaceous materials were characterized using field-emission scanning electron microscopy (FESEM, Hitachi SU6600, Japan) and energy dispersed X-ray spectroscopy (EDX, Oxford Instruments, USA) mounted on the FESEM. High-resolution transmission electron microscopy (HRTEM) analysis was performed using a H9500 (Hitachi, Japan) electron microscope with an acceleration voltage of 200 kV. Sample preparation for the HRTEM was performed using a focused ion beam (FIB) milling machine

(NB5000, Hitachi, Japan). Nitrogen adsorption-desorption was performed for the pore size distribution using Quantachrome Autosorb iQ gas sorption analyzer (Quantachorme Instruments, USA). The Brunauer–Emmett–Teller (BET) method was used to measure the specific surface area of the resultant materials.

3. Results and Discussion

3.1 Carbon yield of water-based IC-chitin composite

We first characterized the carbon yield of the water-based IC-chitin composite. This was required to determine the correct amount of WO_3 particles to add to the biopolymer mix. The targeted WO_3:C ratio was 1:6 in order to provide a carbon surplus and achieve a stoichiometric reaction during heat treatment. As illustrated in Figure 1, the carbon yield of the mix IC-chitin only was 7.7% when accounting for water evaporation (a weight loss of ~60% around 100 °C). A significant weight loss is observed in the temperature range 200 °C – 400 °C. This is attributed to the escape of volatile products caused by thermal degradation of the biopolymers [34,35]. As the temperature increases, further gradual weight loss is observed due to the elimination of heteroatoms such as hydrogen, nitrogen and oxygen from the carbonaceous material [36]. Previous studies reported that the biopolymers yield to a carbonaceous material having more than 90% carbon at 1000 °C [36–38]. The other elements present in the material are nitrogen, oxygen and hydrogen [36,38,39]. It is important to note that the carbon yield reported above was determined when analyzing the water-based IC-chitin composite. The carbon yield when analyzing this water-based composite was 7.7%. This can be considered low. However, the carbon yield increased to 30.8% if the weight of the water is not taken into account. Water evaporated at around 100 °C. The carbon yield of the IC-chitin mixture is of relevance because it surpasses that of IC or chitin by themselves [40,41]. Our hypothesis is that the strong intermolecular binding of iota-carrageenan and chitin prevents the release of the carbon atoms to some extent during the thermal degradation, which results in the higher carbon yield of the IC-chitin mix. Further study is needed to fully understand the thermal degradation process of such biopolymer composite.

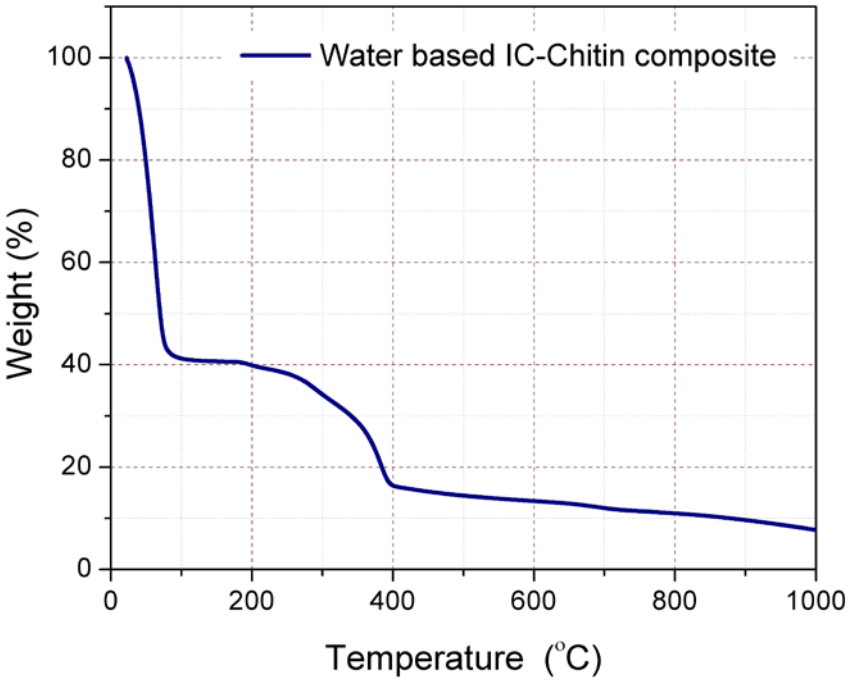

Figure 1: TGA result when heating the water-based IC-chitin composite up to 1000 °C in nitrogen with a heating rate of 5 °C/min. Note how a significant weight loss occurs up to 100 °C due to the evaporation of the water. Further significant weight loss is observed between 200 °C and 400 °C. This is due to the escape of the volatile products during thermal decomposition of the biopolymers.

3.2 Effect of Temperature on the synthesis of Tungsten carbide

The XRD patterns of the carbonaceous materials obtained from the heat treatment of the PCP (the gel-like, water-based composite of IC, chitin and WO_3 particles) at different temperatures are shown in Figure 2a. Major peaks are identified at the 2θ angles of 31.7°, 35.9°, 48.6°, 64.4° and 66.1° which are indexed to the (001), (100), (101), (110) and (002) crystal planes of hexagonal tungsten carbide (WC) respectively (ICDD PDF number 01-072-0097). The other peaks in the XRD patterns correspond to tungsten hemicarbide (W_2C) and tungsten (W) as matched to the ICDD PDF numbers 01-071-6322 and 00-001-1204 respectively. No presence of carbide is observed in XRD patterns for 750 °C and 900 °C. At 750 °C, the peaks in the diffraction pattern correspond to WO_3 and $W_{18}O_{49}$, which infers that WO_3 was partially reduced to its metastable oxide $W_{18}O_{49}$. At this state, the nanoparticles were expected to be surrounded by the amorphous carbon that resulted from the carbonization of the biopolymers at lower temperatures (350 – 600 °C). WO_3 and $W_{18}O_{49}$ were completely reduced by the surrounding carbon material to metallic tungsten at 900 °C. At 960 °C, metallic tungsten is the dominant material and small amounts of WC and its hemicarbide form W_2C are observed. This indicates that the synthesis reaction of WC started in the temperature range between 900 °C-960 °C. The intensity of the peaks for WC increases proportional to the temperature, whereas the peak intensity of W decreases. Increasing the temperature further results in the disappearance of metallic tungsten at1300 °C and 1450 °C. The presence of W_2C hemicarbide phase also decreases with the increase in temperature as observed by the diminishing peaks at temperatures 960 °C – 1450 °C.

To better estimate the relative proportion of the different phases in the material, the ratio between the sum of the peak intensity of a particular phase (I_n) and the sum of the peak intensities from all phases (I_{total}) is plotted in Figure 2b. As the temperature increases, WC rapidly becomes the dominant phase. At 1300 °C, the relative amount of metallic tungsten decreases down to zero which indicates complete carburization of W. A small amount of W_2C is still present in the samples treated at 1300 °C. An even smaller amount is found when heating to 1450 °C. We could not test higher temperatures due to limitations in our experimental setup. However, we expect hemicarbide to completely disappear at temperatures above 1600 °C [42]. The result from this work is the obtainment of a 98.2% pure WC. The other 1.8% is W_2C. A WC purity of 99% is obtained when heating at 1450 °C. This result is significant because it shows that the proposed process consumes less energy that current approaches; in which the required temperature to obtain a carbide with up to 99% purity is up to 1800 °C [43].

Using XRD, we analyzed the formation of WC through the solid-solid reaction between WO_3 and carbon. This analysis is in good agreement with the reported theory [44]. From the TGA results in Figure 1, it is evident that the IC-chitin biopolymer complex decomposes to a carbon rich material in the temperature range between 350 °C and 600 °C. This carbon excess causes a reduction of the WO_3 nanoparticles to metallic W [45,46]. During such reduction, WO_3 transforms into several other oxide forms such as WO_{3-x} and WO_2. The oxygen molecules present in these oxides react with the surrounding carbon to form carbon monoxide (CO) and carbon dioxide (CO_2) [42]. Once the reduction process is complete and the temperature is further increased above 900 °C, W reacts with the surrounding carbon to form WC. During this carburization process, W_2C is also formed, likely due to the carbon deficiency in the reaction [44]. W_2C can be further carburized to WC at higher temperature in the presence of carbon [33]. The following reactions are expected to occur during the whole process [33,44]:

$$WO_3 + C \rightarrow WO_2 + CO\ (g) \quad \text{Equation 1}$$

$$WO_3 + CO\ (g) \rightarrow WO_2 + CO_2(g) \quad \text{Equation 2}$$

$$WO_2 + 2CO\ (g) \rightarrow W + 2CO_2\ (g) \quad \text{Equation 3}$$

$$CO_2(g) + C \rightarrow 2CO(g) \quad \text{Equation 4}$$

$$W + C \rightarrow WC \quad \text{Equation 5}$$

$$2W + C \rightarrow W_2C \quad \text{Equation 6}$$

$$W_2C + C \rightarrow 2WC \quad \text{Equation 7}$$

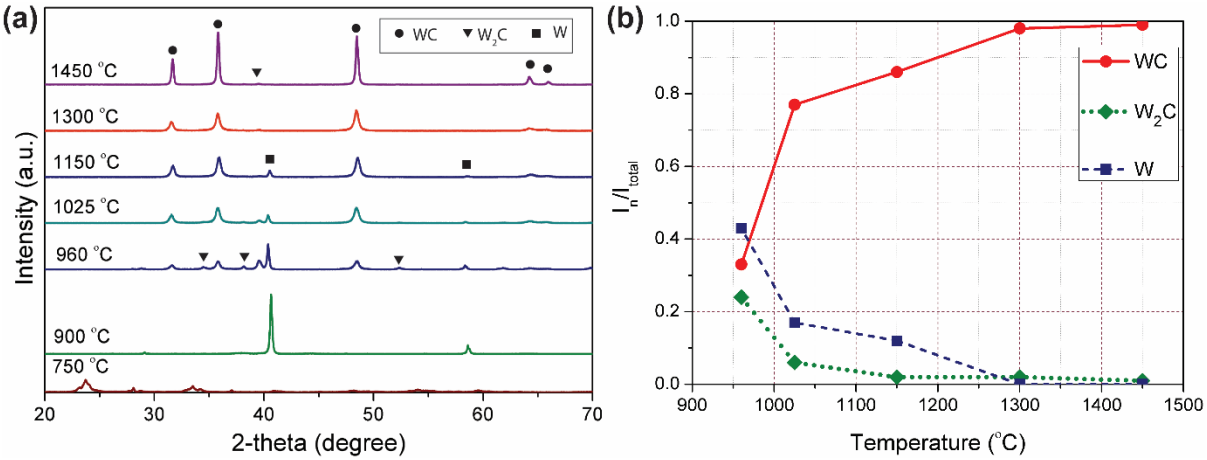

Figure 2: (a) XRD plots illustrating the effect of final temperature in the composition of the resulting carbonaceous materials. The PCP composite was heat treated to different final temperatures in a nitrogen atmosphere for 3 hours. At least 3 independent experiments were performed for each temperature and reproducible results were obtained. (b) Plot of I_n/I_{total} against the reaction temperature. Note the obtainment of a 98.2% pure WC at temperature of 1300 °C and further increase in purity to 99% as the temperature increases to 1450 °C.

3.3 Effect of Dwell Time on synthesis of Tungsten carbide

The impact of different dwell times at the final temperature of 1300 °C is illustrated in Figure 3. A dwell time of zero is when the furnace was turned off immediately after reaching 1300 °C. Mostly WC, with varying amounts of metallic W and W_2C, can be observed in this case. A small amount of the metastable phase of tungsten oxide (W_5O_{14}) is also observed, which indicates the incomplete reduction of WO_3 to W. As the dwell time increases to 15 minutes, tungsten oxide is eliminated and the intensity of the metallic W is decreased in a significant amount. Metallic W can be eliminated from the material when the dwell time is equal to and longer than 3 hours. The use of longer dwell times yields incremental improvements to the purity of WC in the material, from 98.2% at 3 hours to 99% at 9 hours. Our hypothesis is that major carburization reactions between the precursors are completed within 3 hours after reaching 1300 °C. At that point, there is almost no material available for reaction in the sample. Furthermore, the energy available for reaction remained constant, as the temperature did not increase. Hence, no significant improvement in the proportional quantity of WC was observed after 3 hours. A dwell time longer than 3 hours does not seem to be necessary. This is beneficial because a shorter dwell time will be enough to obtain a material with small grain size, high porosity and high specific surface area as characterized in the later sections.

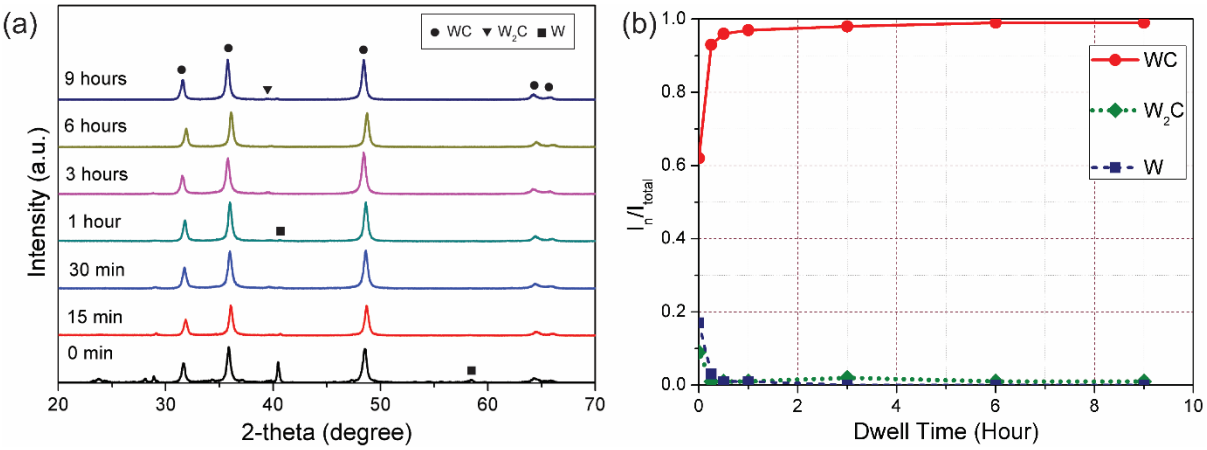

Figure 3: (a) The effect of dwell time at 1300 °C on the composition of the carbonaceous material derived by heat treating the PCP. (b) Plot of I_n/I_{total} versus dwell time. Note that a pure WC can be obtained at the dwell time of 3 hours.

3.4 Microstructure characterization:

Electron microscopy (EM) was used to characterize the grain size obtained in the sample heat treated at 1300 °C for 3 hours. The microstructure is characterized by particle agglomerates and a porous nature (FESEM results, Figure 4a). The size of agglomerates ranges from tens of nanometers to 800 nm. Further analysis using HRTEM resulted in the characterization of the carbide particle size in the order of tens of nanometers (Figure 4b). The nature of the sample was confirmed to be WC by a) determining the d-spacing between lattice fringes, and b) by electron diffraction. The d-spacing was 0.25 nm and is attributed to the (100) plane of hexagonal WC (Figure 4c). The results from electron diffraction match with the WC lattice z-plane of [001] (Figure 4c inset).

The grain size of the WC was estimated from the XRD patterns using the Scherrer equation. This equation is only valid for grain sizes smaller than 100 nm [47] and is thus applicable to the material presented here. The Scherrer equation (equation 8) relates the average grain size D, to the wavelength of X-ray λ, the Bragg angle θ, the half width of the diffraction peak B and a constant k, which is generally taken as 1.

$$D = \frac{k\lambda}{B\cos\theta} \qquad \text{Equation 8}$$

Using equation 8, the grain size was plotted for different temperatures and dwell times. Results are presented in Figure 4e and 4f respectively. The grain size of WC increases from 17.5 nm at 960 °C to 43.3 nm at 1450 °C. This supports the findings of previous authors on the fact that grain size increases with increasing temperature [48]. In contrast, there is almost no change in grain size with the increase in the dwell time. As long as the temperature remains at 1300 °C, the grain size remains constant at around 20 nm for different dwell times. Hence, between temperature and dwell time, the former is the most important process parameter to control grain size. Small grain sizes are desired to improve the mechanical strength of the material [49]. Ongoing work is on characterizing the mechanical properties of the materials presented here.

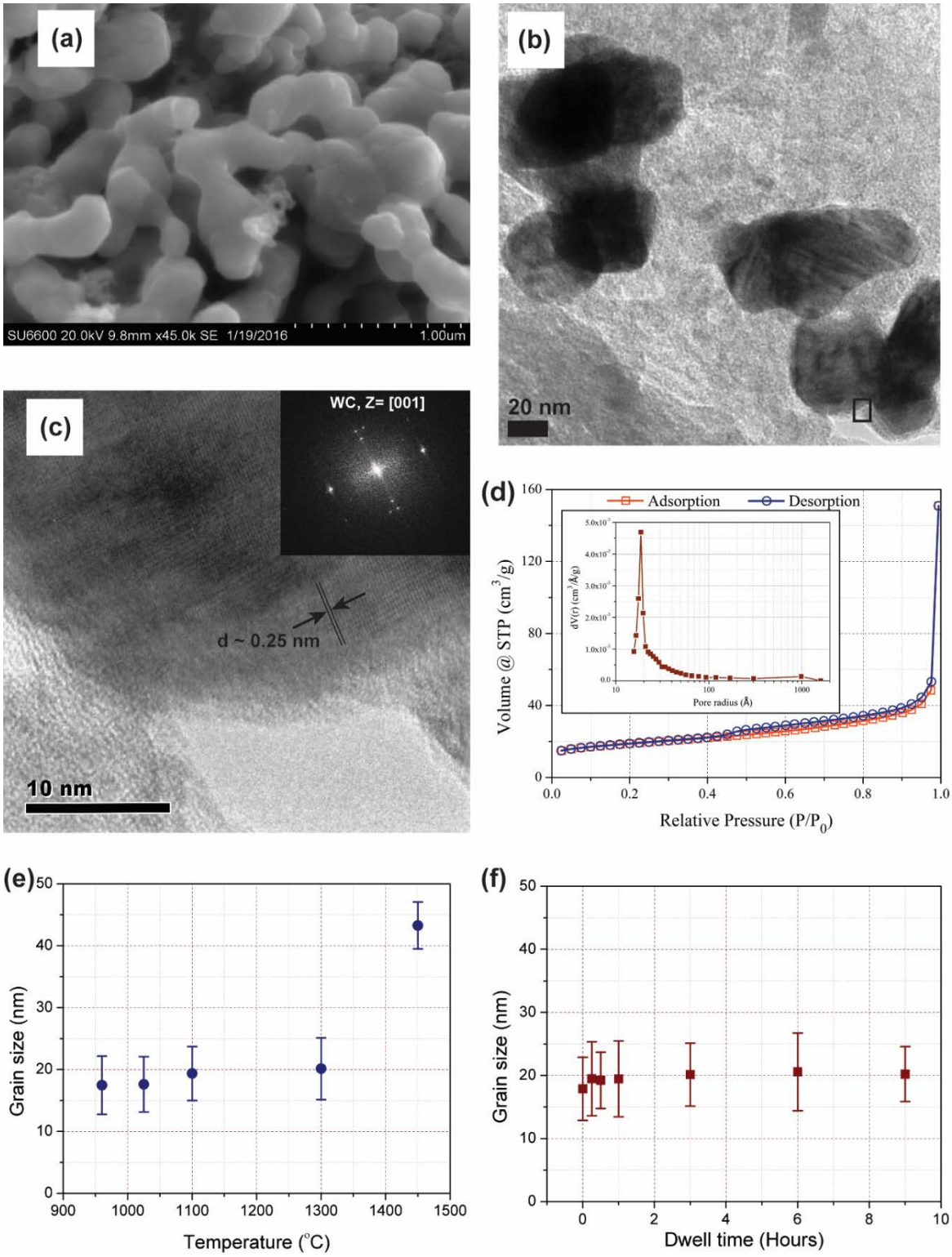

Figure 4: Characterization of WC synthesized at 1300 °C with a dwell time of 3 hours and heating rate of 5 °C/min. (a) FESEM results showing agglomeration of the particles. (b) HRTEM results showing the size of the WC particles (dark regions). The rectangle in the lower right denotes the area of detailed analysis to validate material composition (c) the d-spacing of 0.25 nm between lattice structures confirm the presence of WC. The electron diffraction pattern

is shown in the inset. (d) Nitrogen adsorption desorption isotherm. The pore size distribution in the sample is shown in the inset. Pore size ranging from 3 nm to 120 nm is observed. The grain size as calculated from XRD data using equation 8 (e) at different temperatures for a dwell time of 3 hours, and (f) for different dwell times at 1300 °C.

The nitrogen adsorption desorption isotherm is shown in Figure 4d. The isotherm is of type II and hysteresis of H3 type, which confirms the formation of particle agglomerates and open pores. The steep slope in high relative pressures ($P/P_0 > 0.8$) suggests the presence of macropores (pore diameter > 50 nm) in the material [50]. Although the pore size ranges from 3 nm to 120 nm, most of the pores present in the material are mesopores, that is, featuring a diameter between 2 and 50 nm (Figure 4d, inset). The total pore volume in the material was measured to be 0.9 cm^3/g. Our hypothesis is that the evaporation of water in the early stage of heat treatment causes the large pores, whereas the escape of gaseous material during carbothermal reduction reaction leads to the formation of the mesopores in the material. The BET surface area of the WC was measured to be 67.03 m^2/g.

3.5 Manufacturing of tungsten carbide pieces:

Molding of the PCP was done as described in the experimental section. The de-molded xerogel and the WC shape resulting from the heat treatment of such xerogel are shown in Figures 5a and 5b respectively. The xerogel was heat treated to 1300 °C for 3 hours in a N_2 atmosphere. The mold featured circles and squares of varying dimensions. These dimensions are specified in the x axis of the plots presented in Figure 5c. The data points labeled as failures in Figure 5c reflect the challenge to obtain geometries with characteristic dimension less than 3 mm. At these dimensions, the PCP could be introduced into the mold and dried, but the PCP xerogel broke during de-molding. Shrinkage occurs both during drying of the de-molded PCP to obtain the xerogel and during heat treatment of the xerogel to derive WC. Shrinkage depends on the geometry of the shape. For circular shapes, a shrinkage of approximately 20% occurred in the transition from PCP to xerogel. Shrinkage of the WC piece with respect to the original mold was 36% Shrinkage of square shapes from PCP to xerogel, at 14%, is slightly less than that observed for circular shapes. The shrinkage of WC square shapes compared to the PCP was 35%, similar to that obtained with circular shapes. The shrinkage in the xerogel is attributed to the evaporation of water. In the case of WC, the cause for shrinkage is the escape of gaseous byproducts during carbonization of the biopolymers and during carbide synthesis. The resulting shapes are fragile because of the highly porous nature of the xerogel and the WC. During the drying process, several cracks appeared in the xerogel due to thermal stress introduced during shrinkage. These cracks transcribed to the WC structures, which is a disadvantage of this process. Further optimization of the heating and cooling ramps will minimize the formation of cracks in the xerogel.

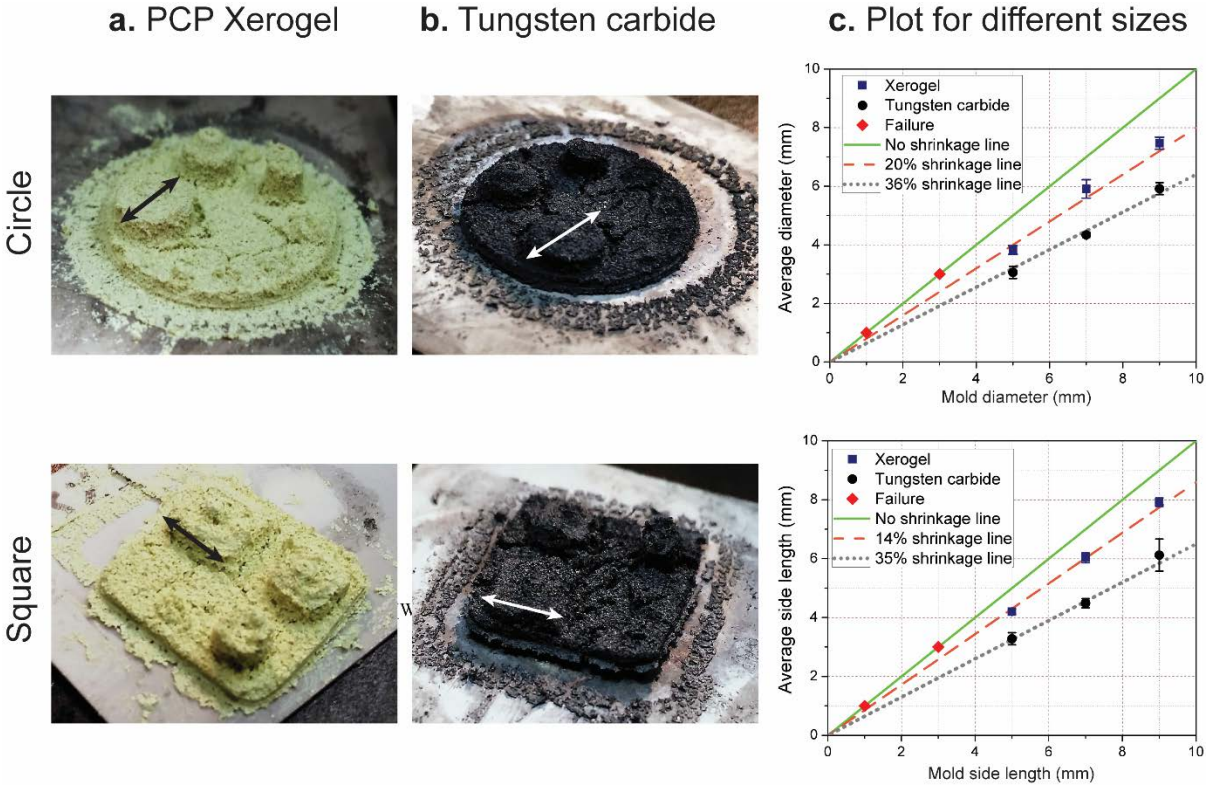

Figure 5: Results for the molding of the WC of circular and square cross section. (a) The molded porous PCP xerogel structure obtained after drying and demolding from the molds. (b) The WC structures obtained by heat treatment of the molded PCP xerogel. The representative mold dimensions are shown with the black and white arrows in the PCP xerogel and WC structures respectively. Note how the WC retained the shape of the xerogel. Features with characteristic dimension of 3 mm or less could not be de-molded successfully. (c) The results of molding of different sizes of the cross sections showing the amount of shrinkage occurred in case of PCP xerogel and WC with respect to mold dimension.

3.6 Advantages and Disadvantages

3.6.1 Renewable resources

The biopolymers used here as carbon precursors are inexpensive and renewable resources. Iota-carrageenan is extracted from red algae and widely used in the food industry as a food thickener. Although the market price varies, carrageenan (CAS 9062-07-1) is significantly less expensive than mesoporous carbon (CAS 1333-86-4) used in the carbide industry (USD$0.5/g vs. $16.45/g as retrieved from Sigma Aldrich 12/7/2016). *Eucheuma* and *Kappaphycus* are two well-known species for the production of iota-carrageenan. The global production of these algae is around 20 million wet tons among which around 9 million tons are cultivated in developing countries [51]. The countries with major contribution to the production of carrageenan are Indonesia, the Philippines, the United Republic of Tanzania, and Malaysia. In these countries, the cultivation of seaweed has a positive socio-economic impact because of short production cycles, low capital cost and simple farming technology that can be conducted by various members of a family. Indeed, seaweed farming has become a source of income in coastal areas that had no previous economic prospects [52].

Chitin is the second most abundant biopolymer in nature, preceded only by cellulose. The annual turnover of chitin is estimated to be $10^{10} – 10^{11}$ tons [53]. The major source of industrial chitin is the exoskeleton of shellfish disposed as waste by the shrimp, lobster and crab industries [54]. According to the United Nations' Food and Agriculture Organization, the world annual production of shrimp alone is around 9.6 million tons, including extraction from the seas and grown in farms [55]. In terms of human consumption of shrimp, around 40% – 50% of the total mass turns out to be waste material [56]. Extensive research to enable the use of the otherwise wasteful shells into a useful commodity is ongoing around the world [56,57]. Powdered chitin from shrimp shells (CAS 1398-61-4) can be purchased at USD$0.59/g.

A disadvantage about the use of carrageenan and chitin is the fact that their extraction involves alkali or acidic washes. For example, dried seaweed is boiled and washed in hot alkali to increase the quality of carrageenan by eliminating the sulphate groups and the minerals from the seaweed [58]. The production of chitin from shrimp shells includes alkali treatment with 4% NaOH for deproteinisation, and acidic treatment using 4% HCl for demineralization [59]. Several studies are ongoing to find alternatives to these chemical extraction methods. For carrageenan extraction, the microwave heating method reduces the use of alkali in a significant amount [60]. For chitin extraction, few biotechnological methods are in development. These employ bacterial fermentation for deproteinisation and demineralization [56,61]. It is also important to note that the amount of carrageenan and chitin required is much higher than the carbon black required for the synthesis of an equivalent amount of carbide. Despite this, the production of chitin and carrageenan demands far less energy than oil extraction and subsequent derivation of carbon black. Furthermore, the price of oil is volatile and dependent on several variables, which are hard to predict. Although the prices of renewable carrageenan and chitin also depend on the market, their price has historically been more constant and their supply stable [51,62].

3.6.2 Synthesis temperature

The traditional WC synthesis methods can be categorized in three categories: high temperature direct carburization, carbothermal reduction reaction and carburization by gaseous hydrocarbon. The high temperature carburization involves fusion of tungsten and carbon around 2800 °C in hydrogen atmosphere [63]. Both carbothermal reduction reaction and carburization by gaseous hydrocarbon include the carburization of tungsten in a temperature range 1400 °C – 1800 °C [14]. All of these traditional processes use temperatures in excess of 1400 °C for the synthesis of WC. Here, we have demonstrated the synthesis of >98% pure WC at temperatures as low as 1300 °C. Lower synthesis temperature implies lower energy required in the process. Together with the choice of precursors, this makes our process more energy efficient than the traditional methods.

3.6.3 Porosity

The WC synthesized here is mostly mesoporous and features a BET surface area of 67.03 m^2/g. This value is higher than the surface area of commercial grade WC (BET < 10 m^2/g) synthesized using carbon black and tungsten precursors [64]. We expect the porosity of the matrix to change depending on the composition of the precursor, mixing protocols and heating

rate during treatment. Ongoing work focuses on understanding the specific impact of these processing parameters on the WC. Nevertheless, materials that have specific surface area and porosity similar to the WC presented here have been used as catalytic materials [65] and for sensor applications [66]. Other applications include energy absorbers and high temperature filters. WC with higher porosity and surface area (BET > 100 m^2/g) can be synthesized using the template method [67]. In such method, a sacrificial material in the matrix is dissolved. However, removal of the template generally requires washing with highly corrosive agents such as hydrofluoric acid [67]. This leads to an increase on processing costs due to the need for highly selective sacrificial materials and the precautions that must be taken when working with hazardous reagents. Further investigation of the process presented here can lead to materials with high surface area. These would be derived using renewable materials and a less expensive, less dangerous and more environmental-friendly process.

4. Conclusion

In this work, we presented a sustainable, energy efficient and environment-friendly method for WC synthesis. A renewable biopolymer-complex was used as the carbon source. This replaces petroleum-based carbon precursors. Porous WC was synthesized by heat-treating a biopolymer-tungsten oxide composite (PCP) at 1300 °C for 3 hours. This temperature is lower than the temperature used in traditional methods of WC synthesis. Grain size of the WC at this condition was estimated to be around 20 nm. Such small grain size is expected to yield high mechanical strength of the material. The WC obtained here is mostly mesoporous, although a small number of macropores were present in the material. The BET surface area was measured as 67.03 m^2/g. Such porosity, surface area and small grain size are preferable for potential catalysts, fuel cell, structural filters and battery applications. Manufacturability of the PCP was demonstrated by using gel casting to fabricate squares and cylinders of different sizes. Although shrinkage of the fabricated components does occur, the geometry is maintained throughout heat treatment. Ongoing work is on further understanding the cause of the cracks developed in the components and optimizing the process to manufacture porous WC pieces. Future work will include tailoring the rheology of the PCP to enable its use in the additive manufacturing of complex shapes that yield complex WC geometries. The ultimate goal is the development of structural cellular materials with energy functionality, which are manufactured using energy efficient processes and sustainable resources.

Acknowledgements

The authors are grateful to Dr. Taghi Darroudi from the Electron Microscopy Laboratory in Clemson University for his help in sample preparation and advice during imaging; and to Dr. Kimberly Ivey from the Analytical Measurement Laboratory in Clemson University for facilitating TGA studies.

References

[1] S. Shanmugam, D.S. Jacob, A. Gedanken, Solid state synthesis of tungsten carbide nanorods and nanoplatelets by a single-step pyrolysis, J. Phys. Chem. B. 109 (2005)

19056–19059.

[2] T.Y. Kosolapva, Carbide Properties, Production, an Application, Plenum Press, New York, 1971.

[3] A.S. Kurlov, A.I. Gusev, Tungsten Carbides: Structure, Properties and Application in Hardmetals, Spinger Science and Business Media, 2013.

[4] N. Ji, T. Zhang, M. Zheng, A. Wang, H. Wang, X. Wang, J.G. Chen, Direct catalytic conversion of cellulose into ethylene glycol using nickel-promoted tungsten carbide catalysts, Angew. Chemie - Int. Ed. 47 (2008) 8510–8513. doi:10.1002/anie.200803233.

[5] M. Rosenbaum, F. Zhao, U. Schröder, F. Scholz, Interfacing electrocatalysis and biocatalysis with tungsten carbide: A high-performance, noble-metal-free microbial fuel cell, Angew. Chemie - Int. Ed. 45 (2006) 6658–6661. doi:10.1002/anie.200602021.

[6] H. Meng, P.K. Shen, Tungsten carbide nanocrystal promoted Pt/C electrocatalysts for oxygen reduction, J. Phys. Chem. B. 109 (2005) 22705–22709. doi:10.1021/jp054523a.

[7] D. Garg, P.N. Dyer, Tungsten Carbide Erosion Resistant Coating for Aerospace Components, Mater. Res. Soc. Proc. 168 (1989) 213.

[8] S. Decker, a Löfberg, J. Bastin, a Frennet, Study of the preparation of bulk tungsten carbide catalysts with C2H6/H2 and C2H4/H2 carburizing mixtures, Catal. Letters. 44 (1997) 229–239. doi:10.1023/A:1018985227289.

[9] A. Löfberg, A. Frennet, G. Leclercq, L. Leclercq, J.M. Giraudon, Mechanism of WO3 Reduction and Carburization in CH4/H2 Mixtures Leading to Bulk Tungsten Carbide Powder Catalysts, J. Catal. 189 (2000) 170–183. doi:10.1006/jcat.1999.2692.

[10] J.B. Claridge, A.P.E. York, A.J. Brungs, C. Marquez-Alvarez, J. Sloan, S.C. Tsang, M.L.H. Green, New Catalysts for the Conversion of Methane to Synthesis Gas: Molybdenum and Tungsten Carbide, J. Catal. 180 (1998) 85–100. doi:10.1006/jcat.1998.2260.

[11] X.G. Yang, C.Y. Wang, Nanostructured tungsten carbide catalysts for polymer electrolyte fuel cells, Appl. Phys. Lett. 86 (2005) 1–3. doi:10.1063/1.1941473.

[12] M. Rosenbaum, F. Zhao, M. Quaas, H. Wulff, U. Schröder, F. Scholz, Evaluation of catalytic properties of tungsten carbide for the anode of microbial fuel cells, Appl. Catal. B Environ. 74 (2007) 261–269. doi:10.1016/j.apcatb.2007.02.013.

[13] Y. Hara, N. Minami, H. Matsumoto, H. Itagaki, New synthesis of tungsten carbide particles and the synergistic effect with Pt metal as a hydrogen oxidation catalyst for fuel cell applications, Appl. Catal. A Gen. 332 (2007) 289–296. doi:10.1016/j.apcata.2007.08.030.

[14] OECD SIDS, Tungsten Carbide, 2005.

[15] J. Barker, M.Y. Saidi, J.L. Swoyer, A Carbothermal Reduction Method for the Preparation of Electroactive Materials for Lithium Ion Applications, J. Electrochem. Soc. 150 (2003) A684. doi:10.1149/1.1568936.

[16] X. Guo, L. Zhu, W. Li, H. Yang, Preparation of SiC powders by carbothermal reduction with bamboo charcoal as renewable carbon source, J. Adv. Ceram. 2 (2013) 128–134. doi:10.1007/s40145-013-0050-4.

[17] J. Wang, R. Ishida, T. Takarada, Carbothermal reactions of quartz and kaolinite with coal char, Energy and Fuels. 14 (2000) 1108–1114. doi:10.1021/ef000084x.

[18] C. Czosnek, J.F. Janik, Z. Olejniczak, Silicon carbide modified carbon materials. Formation of nanocrystalline SiC from thermochemical processes in the system coal tar pitch/poly(carbosilane), J. Clust. Sci. 13 (2002) 487–502. doi:10.1023/A:1021171511204.

[19] a. Alizadeh, E. Taheri-Nassaj, N. Ehsani, Synthesis of boron carbide powder by a carbothermic reduction method, J. Eur. Ceram. Soc. 24 (2004) 3227–3234. doi:10.1016/j.jeurceramsoc.2003.11.012.

[20] M. Narisawa, H. Yasuda, R. Mori, H. Mabuchi, K. Oka, Y.-W. Kim, Silicon carbide particle formation from carbon black ― polymethylsilsesquioxane mixtures with melt pressing, J. Ceram. Soc. Japan. 116 (2008) 121–125.

[21] N.Z. Muradov, T.N. Veziroğlu, From hydrocarbon to hydrogen-carbon to hydrogen economy, Int. J. Hydrogen Energy. 30 (2005) 225–237. doi:10.1016/j.ijhydene.2004.03.033.

[22] T.A. Ruble, Carbon Black from Petroleum Oil, in: Refin. Pet. Chem., ACS Publication, Houston, TX, 1970: pp. 264–270.

[23] U.S. Energy Information Administration, How much oil is consumed in the United States?, (2016). https://www.eia.gov/tools/faqs/faq.cfm?id=33&t=6.

[24] J.S. Prener, N.Y. Schenectady, Method of making silicon carbide, 3085863, 1963.

[25] Z. Schnepp, S.C. Wimbush, M. Antonietti, C. Giordano, Synthesis of highly magnetic iron carbide nanoparticles via a biopolymer route, Chem. Mater. 22 (2010) 5340–5344. doi:10.1021/cm101746z.

[26] B. Wang, C. Tian, L. Wang, R. Wang, H. Fu, Chitosan: a green carbon source for the synthesis of graphitic nanocarbon, tungsten carbide and graphitic nanocarbon/tungsten carbide composites., Nanotechnology. 21 (2010) 025606. doi:10.1088/0957-4484/21/2/025606.

[27] M.W.R. Holgate, T. Schoberl, S.R. Hall, A novel route for the synthesis of nanocomposite tungsten carbide–cobalt using a biopolymer as a carbon source, J. Sol-Gel Sci. Technol. 49 (2008) 145–149. doi:10.1007/s10971-008-1869-y.

[28] A. Ilnicka, P.A. Gauden, A.P. Terzyk, J.P. Lukaszewicz, Nano-Structured Carbon Matrixes Obtained from Chitin and Chitosan by a Novel Method, J. Nanosci. Nanotechnol. 15 (2015) 1–9. doi:10.1166/jnn.2015.10839.

[29] Y. Fan, X. Yang, B. Zhu, P.F. Liu, H.T. Lu, Micro-mesoporous carbon spheres derived from carrageenan as electrode material for supercapacitors, J. Power Sources. 268 (2014) 584–590. doi:10.1016/j.jpowsour.2014.06.100.

[30] E. V Shumilina, Y. a Shchipunov, Chitosan – Carrageenan Gels, Colloid. J. 64 (2002) 372–378.

[31] A. Bartkowiak, D. Hunkeler, Carrageenan-oligochitosan microcapsules: Optimization of the formation process, Colloids Surfaces B Biointerfaces. 21 (2001) 285–298. doi:10.1016/S0927-7765(00)00211-3.

[32] N. Keller, B. Pietruszka, V. Keller, A new one-dimensional tungsten carbide nanostructured material, Mater. Lett. 60 (2006) 1774–1777. doi:10.1016/j.matlet.2005.12.017.

[33] M. Sakaki, M.S. Bafghi, J. Vahdati Khaki, Q. Zhang, F. Saito, Conversion of W2C to WC phase during mechano-chemical synthesis of nano-size WC-Al2O3 powder using WO3-2Al-(1 + x)C mixtures, Int. J. Refract. Met. Hard Mater. 36 (2013) 116–121. doi:10.1016/j.ijrmhm.2012.08.002.

[34] L. Zeng, C. Qin, L. Wang, W. Li, Volatile compounds formed from the pyrolysis of chitosan, Carbohydr. Polym. 83 (2011) 1553–1557. doi:10.1016/j.carbpol.2010.10.007.

[35] J.W. Rhim, L.F. Wang, Preparation and characterization of carrageenan-based nanocomposite films reinforced with clay mineral and silver nanoparticles, Appl. Clay Sci. 97-98 (2014) 174–181. doi:10.1016/j.clay.2014.05.025.

[36] E. Raymundo-Piñero, M. Cadek, F. Béguin, Tuning Carbon Materials for Supercapacitors by Direct Pyrolysis of Seaweeds, Adv. Funct. Mater. 19 (2009) 1032–1039. doi:10.1002/adfm.200801057.

[37] A. Ilnicka, M. Walczyk, J.P. Lukaszewicz, The fungicidal properties of the carbon materials obtained from chitin and chitosan promoted by copper salts, Mater. Sci. Eng. C. 52 (2015) 31–36. doi:10.1016/j.msec.2015.03.037.

[38] Y. Qiao, S. Chen, Y. Liu, H. Sun, S. Jia, J. Shi, C. Marcus, Y. Wang, X. Hou, Pyrolysis of chitin biomass : TG – MS analysis and solid char residue characterization, Carbohydr. Polym. 133 (2015) 163–170. doi:10.1016/j.carbpol.2015.07.005.

[39] Y. Gao, X. Chen, J. Zhang, N. Yan, Chitin-Derived Mesoporous, Nitrogen-Containing Carbon for Heavy-Metal Removal and Styrene Epoxidation, Chempluschem. 80 (2015) 1556–1564. doi:10.1002/cplu.201500293.

[40] S.F. Soares, T. Trindade, A.L. Daniel-Da-Silva, Carrageenan-Silica Hybrid Nanoparticles Prepared by a Non-Emulsion Method, Eur. J. Inorg. Chem. 2015 (2015) 4588–4594. doi:10.1002/ejic.201500450.

[41] J.L. Shamshina, G. Gurau, L.E. Block, L.K. Hansen, C. Dingee, A. Walters, R.D. Rogers, Chitin–calcium alginate composite fibers for wound care dressings spun from ionic liquid solution, J. Mater. Chem. B. 2 (2014) 3924. doi:10.1039/c4tb00329b.

[42] R. Koc, S.K. Kodambaka, Tungsten carbide (WC) synthesis from novel precursors, J. Eur. Ceram. Soc. 20 (2000) 1859–1869.

[43] M.J. Hudson, J.W. Peckett, P.J.F. Harris, Low-Temperature Sol - Gel Preparation of Ordered Nanoparticles of Tungsten Carbide / Oxide, (2005) 5575–5578.

[44] P. Hoier, Effect of Carbon Sources and Carbonaceous Atmospheres on the Effective Synthesis of Nanostructured Tungsten Carbide Powders, Chalmers University of Technology, 2014.

[45] G. Leclercq, M. Kamal, J.M. Giraudon, P. Devassine, L. Feigenbaum, L. Leclercq, A. Frennet, J.M. Bastin, A. Lofberg, S. Decker, M. Dufour, Study of the preparation of bulk powder tungsten carbides by temperature programmed reaction with CH4+H2 mixtures, J. Catal. 158 (1996) 142–169. doi:10.1006/jcat.1996.0015.

[46] D.S. Venables, M.E. Brown, Reduction of tungsten oxide with carbon monooxide, Thermochim. Acta. 291 (1997) 131–140.

[47] L. Alexander, H.P. Klug, Determination of crystallite size with the x-ray spectrometer, J. Appl. Phys. 21 (1950) 137–142. doi:10.1063/1.1699612.

[48] Z.Z. Fang, X. Wang, T. Ryu, K.S. Hwang, H.Y. Sohn, Synthesis, sintering, and mechanical properties of nanocrystalline cemented tungsten carbide - A review, Int. J.

Refract. Met. Hard Mater. 27 (2009) 288–299. doi:10.1016/j.ijrmhm.2008.07.011.

[49] V. Richter, M. Ruthendorf, On hardness and toughness of ultra ® ne and nanocrystalline hard materials, Int. J. Refract. Met. Hard Mater. 17 (2000) 141–152.

[50] K. Sing, The use of nitrogen adsorption for the characterisation of porous materials, Colliods Surfaces A Physiochemical Eng. Asp. 187 (2001) 3–9.

[51] D. Valderrama, J. Cai, N. Hishamunda, N. Ridler, Social and economic dimensions of carrageenan seaweed farming: a global synthesis, 2013.

[52] D.J. McHugh, A Guide to the Seaweed Industry, 2003. doi:ISBN 92-5-104958-0.

[53] K. Gopalan Nair, A. Dufresne, Crab shell chitin whisker reinforced natural rubber nanocomposites. 1. Processing and swelling behavior, Biomacromolecules. 4 (2003) 657–665. doi:10.1021/bm020127b.

[54] D.H. Bartlette, F. Azam, Chitin, Cholera, and Competence, Science (80-.). 310 (2005) 1775–1778.

[55] R. Gillett, Global study of shrimp fisheries, Fish. Bethesda. 475 (2008) 331 pp.

[56] W. Arbia, L. Arbia, L. Adour, A. Amrane, Chitin extraction from crustacean shells using biological methods -A review, Food Technol. Biotechnol. 51 (2013) 12–25.

[57] S.L. Wang, T.J. Chang, T.W. Liang, Conversion and degradation of shellfish wastes by Serratia sp. TKU016 fermentation for the production of enzymes and bioactive materials, Biodegradation. 21 (2010) 321–333. doi:10.1007/s10532-009-9303-x.

[58] G. Hernandez-Carmona, Conventional and alternative technologies for the extraction of algal polysaccharides, 2013. doi:10.1533/9780857098689.3.475.

[59] G.T. Kjartansson, S. Zivanovic, K. Kristbergsson, J. Weiss, Sonication-Assisted Extraction of Chitin from North Atlantic Shrimps (Pandalus borealis), J. Agric. Food Chem. 54 (2006) 5894–5902. doi:10.1021/jf060646w.

[60] S.F. Uy, A.J. Easteal, M.M. Farid, R.B. Keam, G.T. Conner, Seaweed processing using industrial single-mode cavity microwave heating: A preliminary investigation, Carbohydr. Res. 340 (2005) 1357–1364. doi:10.1016/j.carres.2005.02.008.

[61] M.S. Rao, J. Muñoz, W.F. Stevens, Critical factors in chitin production by fermentation of shrimp biowaste, Appl. Microbiol. Biotechnol. 54 (2000) 808–813. doi:10.1007/s002530000449.

[62] G.A.F. Roberts, THIRTY YEARS OF PROGRESS IN CHITIN AND CHITOSAN, Prog. Chem. Appl. Chitin. 13 (2008) 7–15.

[63] Gmelin, Tungsten, Supplement A 5b, in: Gmelin Handb. Inorg. Organomet. Chem., Springer Verlag, Berlin, 1993: pp. 131–154.

[64] H. Chhina, S. Campbell, O. Kesler, High surface area synthesis, electrochemical activity, and stability of tungsten carbide supported Pt during oxygen reduction in proton exchange membrane fuel cells, J. Power Sources. 179 (2008) 50–59. doi:10.1016/j.jpowsour.2007.12.105.

[65] Y. Wang, S. Song, P.K. Shen, C. Guo, C.M. Li, Nanochain-structured mesoporous tungsten carbide and its superior electrocatalysis, J. Mater. Chem. 19 (2009) 6149. doi:10.1039/b902744k.

[66] V. Nikolova, I. Nikolov, P. Andreev, V. Najdenov, T. Vitanov, Tungsten carbide-based electrochemical sensors for hydrogen determination in gas mixtures, J. Appl. Electrochem. 30 (2000) 705–710. doi:10.1023/A:1003813210270.

[67] Z. Wu, Y. Yang, D. Gu, Q. Li, D. Feng, Z. Chen, B. Tu, P.A. Webley, D. Zhao, Silica-templated synthesis of ordered mesoporous tungsten carbide/graphitic carbon composites with nanocrystalline walls and high surface areas via a temperature-programmed carburization route, Small. 5 (2009) 2738–2749. doi:10.1002/smll.200900523.